



Characteristic strength and acoustic emission properties of weakly cemented sandstone at different depths under uniaxial compression

Bin Liu^{1,2} · Yixin Zhao^{1,2} · Cun Zhang^{1,2} · Jinlong Zhou^{2,3} · Yutao Li⁴ · Zhuang Sun^{1,2}

Received: 20 May 2021 / Revised: 9 August 2021 / Accepted: 27 August 2021 / Published online: 15 September 2021
© The Author(s) 2021

Abstract As coal mining is extended from shallow to deep areas along the western coalfield, it is of great significance to study weakly cemented sandstone at different depths for underground mining engineering. Sandstones from depths of 101.5, 203.2, 317.3, 406.9, 509.9 and 589.8 m at the Buertai Coal Mine were collected. The characteristic strength, acoustic emission (AE), and energy evolution of sandstone during uniaxial compression tests were analyzed. The results show that the intermediate frequency (125–275 kHz) of shallow rock mainly occurs in the postpeak stage, while deep rock occurs in the prepeak stage. The initiation strength and damage strength of the sandstone at different depths range from 0.23 to 0.50 and 0.63 to 0.84 of peak strength (σ_c), respectively, decrease exponentially and are a power function with depth. The precursor strength ranges from $0.88\sigma_c$ to $0.99\sigma_c$, increases with depth before reaching a depth of 300 m, and tends to stabilize after 300 m. The ratio of the initiation strength to the damage strength (k) ranges from 0.25 to 0.62 and decreases exponentially with depth. The failure modes of sandstone at different depths are tension-dominated mixed tensile-shear failure. Shear failure mainly occurs at the unstable crack propagation stage. The count of the shear failure bands before the peak strength increases gradually, and increases first and then decreases after the peak strength with burial depth. The cumulative input energy, released elastic energy and dissipated energy increase with depth. The elastic release rate ranges from 0.46×10^{-3} to 198.57×10^{-3} J/(cm³ s) and increases exponentially with depth.

Keywords Burial depth · Weakly cemented sandstone · Acoustic emission (AE) · Characteristic strength · Energy evolution · Failure mode

1 Introduction

With the increasing mining depth in the western coalfield of China, water or sand inrush accidents, mining-induced surface cracks, roof falls, and dynamic pressures occur frequently during underground mining (Zhang et al. 2011; Ju et al. 2015; Zhu et al. 2017; Yan et al. 2018; Zhuo et al. 2018; Xue et al. 2020). These phenomena are caused by deformation and failure of the overlying strata rock, and the overlying strata are mainly weakly cemented sandstone. The mechanical properties and deformation behaviors of rock change significantly with increasing depth (He et al. 2005; Xie et al. 2019; Dou et al. 2021). Therefore, it is urgent to carefully analyze the mechanical behaviors and progressive failure processes of weakly cemented sandstone at different depths.

✉ Yixin Zhao
zhaoyx@cumtb.edu.cn

¹ Beijing Key Laboratory for Precise Mining of Intergrown Energy and Resources, China University of Mining and Technology (Beijing), Beijing 100083, China
² School of Energy and Mining Engineering, China University of Mining and Technology (Beijing), Beijing 100083, China
³ CERENA, Pavilhão de Minas, Instituto Superior Técnico, Universidade de Lisboa, Av. Rovisco Pais, 1049-001 Lisbon, Portugal
⁴ School of Mechanics and Civil Engineering, China University of Mining and Technology (Beijing), Beijing 100083, China

The physical properties and mechanical behaviors of deep rocks differ from those of shallow rocks (He et al. 2005; Xie et al. 2019). Researchers have investigated the physical properties of rock and coal at different depths, such as density, compressive strength, Young's modulus, Poisson's ratio, tensile strength, cohesive strength, internal frictional angle, fracture toughness, and permeability (Zhou et al. 2010; Song et al. 2016; Man and Liu 2018; Kang et al. 2019; Zhao et al. 2019; Wang et al. 2020), and the mechanical behaviors of rock and coal at different depths, such as AE parameters, energy evolution, damage evolution, and failure mechanism (Zhang et al. 2019b; Zhao et al. 2019; Jia et al. 2020). However, the physical properties and mechanical behavior of weakly cemented rock are rarely reported. The water or sand inrush accidents, mining-induced surface cracks, roof falls and dynamic pressure are closely related to the evolution of overlying strata rock damage, such as crack initiation, propagation and coalescence (Cai et al. 2004; Martin and Christiansson 2009; Fan et al. 2016). Hoek and Bienawski (1965), Eberhardt et al. (1998), and Cai et al. (2004) classified the stress–strain curve of rock into the crack closure stage, elastic deformation stage, crack stable propagation stage, crack unstable propagation stage and post-peak failure stage according to the active state of microcracks in rock. The starting points of the stable crack growth stage and unstable crack growth stage are the crack initiation strength (σ_{ci}) and damage strength (σ_{cd}), respectively. In the past few decades, there have been many methods, such as the stress–strain method, acoustic emission (AE) method, moving-point regression method and energy dissipation method, which have been suggested to determine the strength thresholds of rock. In the stress–strain method, different parameters for determining σ_{ci} and σ_{cd} , such as volumetric strain (Brace et al. 1966), lateral strain (Lajtai 1974), crack volumetric strain (Martin and Chandler 1994), and instantaneous Poisson's ratio (Diederichs 2007), have been proposed in compression tests. The AE method has also been suggested to investigate the crack initiation and propagation threshold. AE event counts, AE hit numbers, AE energy, and AE ring counts are used to identify σ_{ci} and σ_{cd} (Eberhardt et al. 1998; Chang and Lee 2004; Diederichs et al. 2004; Zhao et al. 2013, 2015; Kim et al. 2015; Moradian et al. 2016). The moving-point regression method was developed by Eberhardt et al. (1998), Chang et al. (2001) and Yang (2016), and they investigated the stress thresholds by using the “sliding-window” approach to move through x and y data sequences and fitting the line within a user-defined interval. Ning et al. (2017) provided a new energy dissipation method to determine crack initiation and propagation strength. The crack initiation and damage threshold have a great difference between different rocks. Martin and

Chandler (1994) found that σ_{ci} and σ_{cd} of Lac du Bonnet granite were 0.4–0.5 and 0.8 of peak strength (σ_c), respectively. Eberhardt et al. (1999) provided that the internal structure of rock had a great influence on σ_{ci} and σ_{cd} and found that σ_{ci} and σ_{cd} of granite were 0.39 and 0.75 σ_c , respectively. Zhao et al. (2013, 2015) investigated the characteristic strength of Beishan granite and found that σ_{ci} and σ_{cd} range from 0.39 to 0.62 and 0.69 to 0.94 of σ_c . Hidalgo and Nordlund (2013) found that the σ_{ci} and σ_{cd} of diorite were 0.51 σ_c and 0.90 σ_c , while the same values of gabbro were 0.58 and 0.80. The σ_{ci} and σ_{cd} of granite were 0.51 σ_c and 0.71 σ_c (Kim et al. 2015). Yang (2016) found that the crack damage threshold of hollow sandstone is approximately 0.689 σ_c .

The analysis of the characteristic strength of hard rock is mostly carried out from previous research, while investigations on the characteristic strength of weakly cemented sandstone at different depths are rarely reported. In this study, uniaxial compression tests of weakly cemented sandstone specimens were carried out using the AE monitoring system and universal testing machine system, and the mechanical properties and AE characteristics of weakly cemented sandstone were analyzed. The characteristic strength of weakly cemented sandstone was analyzed by the AE method and the stress–strain curve method, and the effects of burial depth on the characteristic strength, failure characteristics, and energy evolution were discussed. The results can be a reference for the mechanical properties of weakly cemented sandstone and provide a reference for disaster prevention in deep rock engineering.

2 Experimental setup

2.1 Specimen preparation

The rock cores were taken from BK212 geological drilling in the Buertai Coal Mine, Inner Mongolia Autonomous Region, China. The borehole, with a depth of 597.6 m, has been used to investigate the geological and engineering characteristics of regional strata. The locations of the Buertai Coal Mine and BK212 geological drilling are shown in Fig. 1. Six groups of cores with depths of 101.5, 203.2, 317.3, 406.9, 509.9, and 589.8 m were selected from rock cores at intervals of approximately 100 m. The cores were processed into cylindrical specimens with a diameter of 25 mm, and the specimen height was twice the diameter. Twenty-four specimens were prepared with 4 specimens in each group. The ends and sides of the specimens were polished and shaped according to the International Society for Rock Mechanics (ISRM) suggested methods. Before the test, the P-wave velocities of the rock specimens were

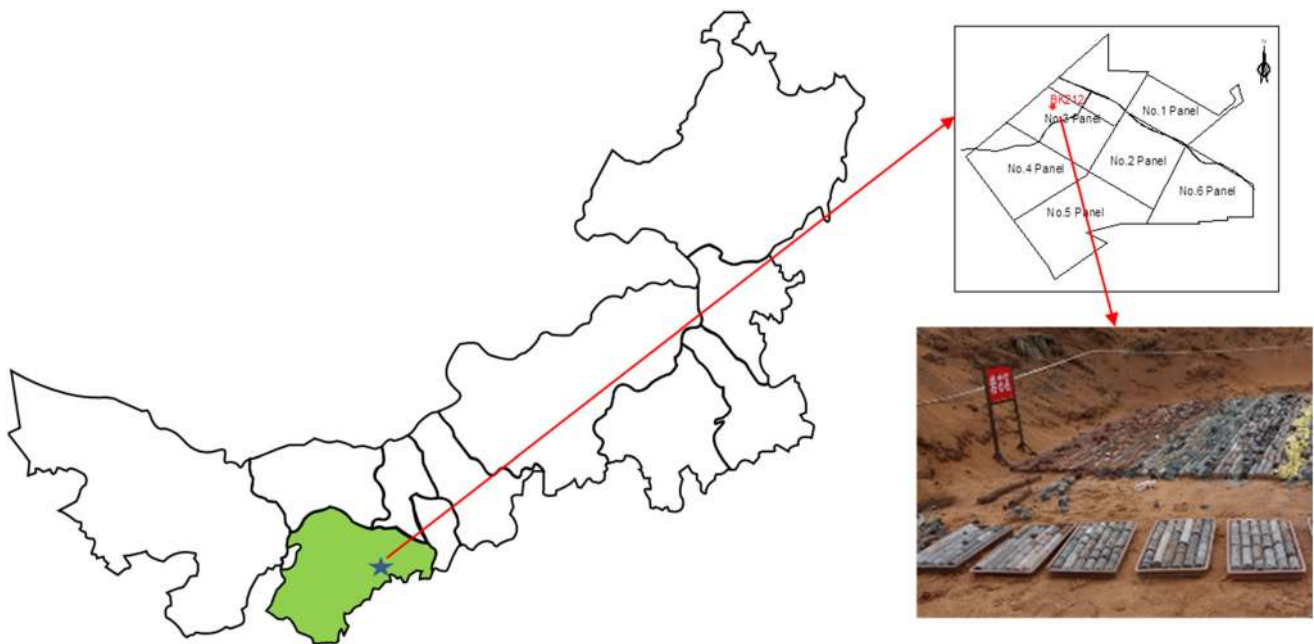


Fig. 1 Location of Buertai coal mine in Inner Mongolia and BK212 geological drilling

obtained. The physical and mechanical properties of the rock specimens are listed in Table 1.

2.2 Experimental system

As shown in Fig. 2, uniaxial compression tests were conducted on weakly cemented sandstone specimens using a rock mechanics test system (Model: WDW-100E) and AE monitoring system (Model: PCI-2). The test system can display and record the load–displacement data in real time, and the ranges of axial load capacity and load rate are 0.4 to 100 kN and 0.005 to 500 mm/min, respectively. The AE monitoring system, manufactured by Physical Acoustic Corporation, can display and record the AE signals during the damage and failure processes simultaneously.

2.3 Experimental methods

The loading rate for uniaxial compression tests was set to 0.50 mm/min by axial displacement control. As shown in Fig. 2, two Nano 30 AE sensors were symmetrically installed in the radial direction along the cylinder central surface. The center frequency of the Nano 30 AE sensor is 140 kHz, and the frequency ranges from 125 to 750 kHz. The threshold and acquisition frequency were set to 40 dB and 1 MHz, respectively. The specimen was fixed on the loading platform of the testing machine by applying an initial load of 0.05 kN during the pre-loading stage. The test system and AE monitoring system were started simultaneously to ensure that the AE signals and load–

displacement data were synchronized. The loading and data acquisition of the two systems were stopped when the rock specimen failed, and the relevant data were stored. Then the damaged specimen was removed and the next specimen was tested.

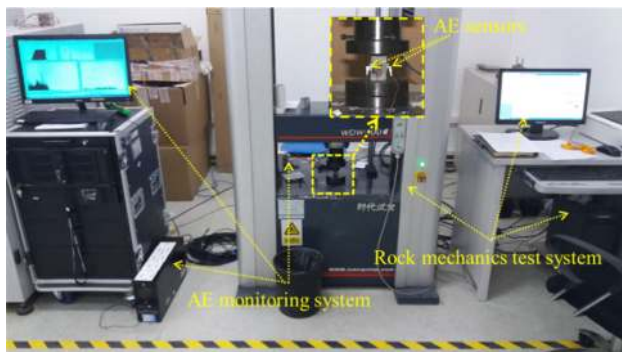
3 Results and discussions

3.1 Physical properties of weakly cemented sandstone at different depths

The weakly cemented sandstone is mainly formed by compaction and cementation of mineral particles and cemented minerals. The physical properties are mainly affected by geological tectonic movement and generally change with burial depth (Li and Li 2017). The distribution of density and P-wave velocity at different depths is shown in Fig. 3. The mean density is distributed mainly among the range of 2270–2580 kg/m³, and its curve has a C-shaped form. The P-wave velocity of rock specimens at different depths is shown in Fig. 3b. The mean P-wave velocity of rock specimens at different depths ranges from 1180 to 1960 m/s. It decreases at the beginning and reaches a minimum of 1180 m/s at a depth of 203.2 m. It further increases at 317.3 m and reaches a maximum of 1960 m/s at a depth of 589.8 m. These results show that the compactness and integrity of sandstone are gradually enhanced with increasing depth, especially at a depth of 589.8 m. However, there are also some discrete values, which are

Table 1 Physical and mechanical properties of rock specimens

Specimen ID	Depth (m)	Diameter (mm)	Height (mm)	Density (10^3 kg/m^3)	P-wave velocity (10^3 m/s)	Mean (10^3 m/s)	Elastic modulus (GPa)	Mean (GPa)	UCS (MPa)	Mean (MPa)
111	101.5	24.54	49.82	2.46	1.07	1.29	0.95	1.45	9.07	11.28
112	101.5	24.74	50.19	2.62	1.22		1.04		7.99	
113	101.5	24.88	49.93	2.63	1.45		1.66		10.40	
114	101.5	24.81	50.14	2.59	1.42		2.15		17.65	
211	203.2	24.62	51.13	2.20	1.15	1.18	0.62	0.78	5.10	6.34
212	203.2	24.34	50.20	2.26	1.14		0.75		5.80	
213	203.2	24.60	50.42	2.28	1.17		0.94		6.92	
214	203.2	24.40	49.93	2.34	1.24		0.80		7.55	
331	317.3	24.93	50.51	2.29	1.58	1.52	2.19	2.08	16.10	16.08
332	317.3	24.85	50.30	2.34	1.44		1.39		11.31	
333	317.3	24.69	49.89	2.31	1.60		2.07		17.19	
334	317.3	24.67	49.40	2.33	1.44		2.67		19.70	
421	406.9	24.90	49.94	2.39	1.84	1.56	4.00	3.56	23.53	22.41
422	406.9	24.87	50.38	2.29	1.55		3.61		21.91	
423	406.9	24.74	50.34	2.31	1.59		2.54		15.69	
424	406.9	24.98	50.27	2.22	1.27		4.09		28.51	
531	509.9	24.76	50.14	2.39	2.02	1.84	8.20	7.63	65.37	59.59
532	509.9	24.90	50.28	2.37	1.70		7.40		39.84	
533	509.9	24.96	50.41	2.34	1.97		8.46		75.66	
534	509.9	24.74	46.46	2.37	1.68		6.47		57.48	
611	589.8	24.87	50.63	2.42	2.04	1.96	3.08	3.60	26.79	26.58
612	589.8	24.96	50.27	2.41	1.99		3.24		28.51	
613	589.8	24.73	50.13	2.44	1.96		3.95		26.64	
614	589.8	24.78	51.24	2.40	1.83		4.12		24.38	

**Fig. 2** Layout of test equipment

caused by the nonorganic mineral composition, grain size, stress conditions and the general integrity of the rock (Galouei and Fakhimi 2015). The density and P-wave velocity of weakly cemented sandstone are lower than those of conventional sandstone due to the low cementation degree (Li et al. 2018).

3.2 Damage and failure characteristics

The uniaxial compressive strength (UCS) and elastic modulus of the rock specimens are listed in Table 1, and the distribution of the UCS and elastic modulus at different depths is shown in Fig. 4. The mean UCS of rock specimens at different depths is mainly distributed among the range of 6.34–59.59 MPa. It decreases at the beginning and reaches a minimum of 6.34 MPa at a depth of 203.2 m. Then, it increases and reaches a maximum of 59.59 MPa at a depth of 509.9 m, which is approximately 9 times that of the sandstone at 203.2 m, and further decreases at a depth of 589.8 m. As shown in Fig. 4b, the elastic modulus of rock specimens at different depths ranges from 0.78 to 7.63 GPa, and the evolution of the elastic modulus is the same as that of the UCS. The elastic modulus reaches a minimum of 0.78 GPa at a depth of 203.2 m, and it reaches a maximum of 7.63 GPa at a depth of 509.9 m, which is approximately 9 times that of sandstone at 203.2 m. The mean UCS and elastic modulus of rock specimens generally increase with burial depth, which is consistent with previous research results (Zhou et al. 2010; Zhang et al.

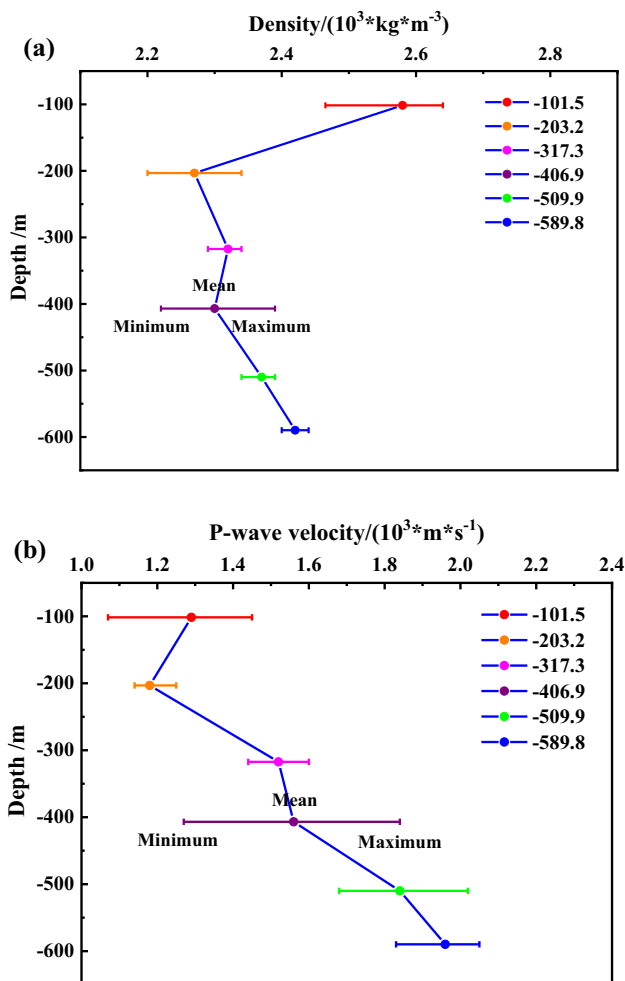


Fig. 3 Distribution of physical properties for rock specimens at different depths **a** density, **b** P-wave velocity

2019b). These nonlinear changes with depth are related to the nonorganic mineral composition, grain size, stress conditions, and general integrity of the rock (Galouei and Fakhimi 2015). These results indicate that the strength and stiffness of the sandstone gradually increases with depth, particularly at a depth of 509.9 m.

The stress and strain were normalized due to the difference in deformation characteristics. Namely, the ratio of stress at any time to peak stress is normalized stress and the ratio of strain at any time to maximum strain is normalized strain. Figure 5 shows the normalized stress–strain curves of typical rock specimens at different depths. According to the crack development pattern, the stress–strain curves of rock specimens at different depths can be divided into the crack closure stage, elastic deformation stage, crack stable propagation stage, crack unstable propagation stage, and postpeak failure stage (Hoek and Bieniawski 1965; Eberhardt et al. 1998). However, compared with the curves of shallow rock specimens, the curves of deep rock

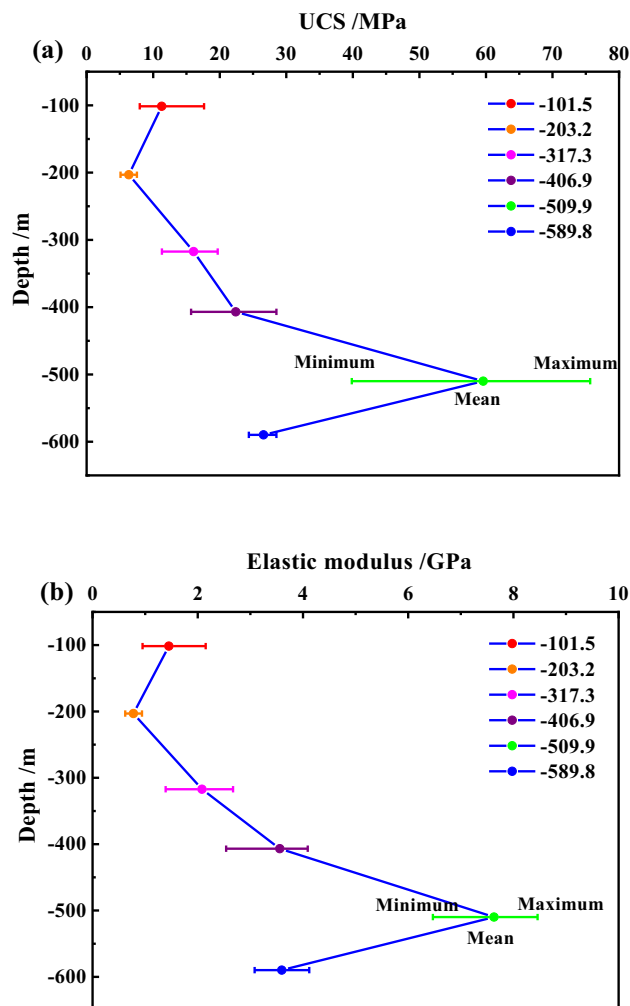


Fig. 4 Distribution of UCS and elastic modulus for rock specimens at different depths **a** UCS, **b** elastic modulus

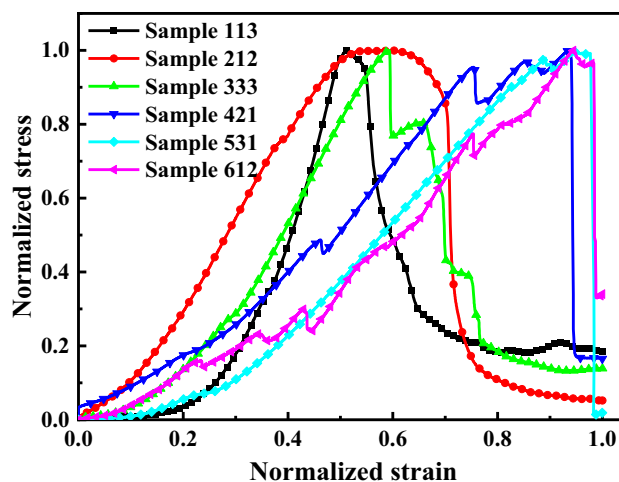


Fig. 5 Normalized stress–strain curves of typical rock specimens at different depths

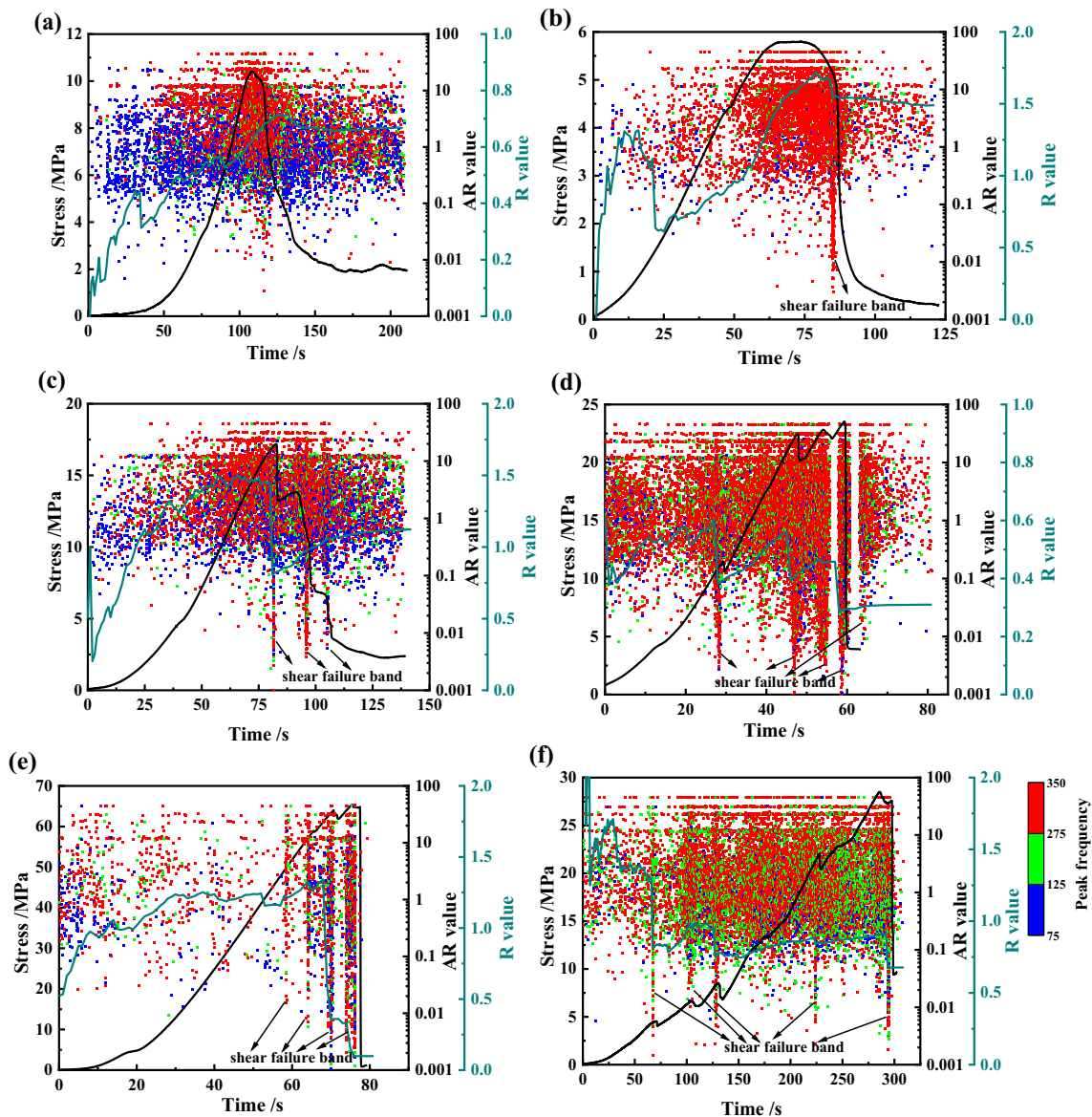


Fig. 6 Curves of AE R value, AR value and stress with time of typical rock specimens at different depths **a** specimen 113, **b** specimen 212, **c** specimen 333, **d** specimen 421, **e** specimen 531, **f** specimen 612

specimens have a long stress adjustment stage and a short postpeak failure stage. The phenomenon shows that deep rock specimens have rheological properties due to high in situ stress. Figure 5 also shows that the normalized peak strain of specimens at different depths is different. The normalized peak strains of sandstone 113, 212, 333, 421, 531 and 612 are 51.29%, 59.80%, 59.27%, 93.59%, 95.15% and 94.57%, respectively. The normalized peak strain of shallow rock specimens above 350 m ranges from 50% to 60%, while that of deep rock below 350 m ranges from 90% to 100%. These changes show that the deep rock specimens have strong brittleness. Thus, dynamic disasters are more likely to occur in deep mining engineering.

3.3 AE characteristics

AE signals are generated in the process of damage and failure of rock, which can be used to analyze the characteristics of crack initiation, propagation and coalescence (Zhao and Jiang 2010; Xie et al. 2011; Zhang et al. 2019a). The AE parameters are obtained from the AE data of each channel, such as the AE hit rate, accumulated hit number, AE energy, accumulated energy, peak frequency, rise time, amplitude, and duration. As shown in Fig. 6, the peak frequency of typical rock specimens ranges from 100 to 350 kHz at different depths, mainly in 75 to 125 kHz and 275 to 325 kHz. Therefore, the frequency bands of 75–125 kHz, 125–275 kHz and 275–325 kHz are defined

as low frequency, intermediate frequency and high frequency, respectively. High and low frequencies are observed throughout the whole loading process, and the intermediate frequency is relatively dense near the peak strength for some rock specimens. However, the intermediate frequency of shallow rock specimens mainly occurs in the postpeak stage, while deep rock specimens are in the prepeak stage. Figure 6 also shows the curves of the R value (ratio of cumulative hit number to cumulative energy) of typical rock specimens at different depths. The increase in the R value indicates that massive low-energy events occur due to crack propagation, while the decrease in the R value indicates that massive high-energy events occur, leading to the generation of macrocracks (Hall et al. 2006; Byun et al. 2012). When the loading begins, the R value rises with fluctuation. During the elastic deformation stage, the R value slowly increases. At the crack stable propagation stage, the R value quickly increases. In the unstable crack propagation stage, the R value rises rapidly. During the postpeak failure stage, the R value tends to stabilize. However, there are some rapid drops in rock specimens at different depths. Shallow sandstone specimens 113 and 212 occur at the prepeak stage and postpeak failure stage, while deep sandstone specimens 333, 421, 531 and 612 occur only at the prepeak stage. In addition, there is a rapid drop before the peak strength for deep specimens 333, 421, 531 and 612, which will be the precursor of rock failure.

3.4 Failure modes

The microfailure mechanism of rock and coal can be investigated by analyzing the AE signals during the damage and failure process. Different types of cracks have different AE waveforms. It is generally believed that tensile cracks have a lower RA value (the ratio of rise time and amplitude) and a higher average frequency AF value (the ratio of count and duration), while shear cracks have a higher RA value and lower AF value, and mixed tensile-shear failure has a lower RA value and lower AF value (Aggelis 2011; Aldahdooh and Bunnori 2013; Carpinteri et al. 2013; Elfergani et al. 2013; Hidalgo and Nordlund 2013; Wang et al. 2016). In this section, the ratio of the AF value and RA value is defined as the AE AR value, and crack types are classified according to their values. When the AR values are higher, they correspond to tensile failure, and when the values are lower, they correspond to shear failure. According to the relevant study about the actual distribution of the AF value and RA value (Aldahdooh and Bunnori 2013), an AR value less than 0.2 is defined as shear failure, more than 1.0 is defined as tensile failure, and 0.2–1.0 is defined as mixed tensile-shear failure.

Figure 6 shows the curves of the AE R value, AR value and stress with time for typical rock specimens at different depths. The evolution of the R value and peak frequency is discussed in Sect. 3.3. The AR value ranges from 0 to 50, which is tension-dominated mixed tensile-shear failure. When loading starts, the AR value is mainly above 0.2, and the peak frequency is mainly at high and low frequencies. During the elastic deformation stage and crack stable propagation stage, the AR value is also mainly above 0.2, and the peak frequency is also mainly at high and low frequencies. At the unstable crack propagation stage, the AR value ranges from 0 to 50 and is distributed in bands. The peak frequency is also mainly at high, intermediate, and low frequencies. During the post-peak failure stage, the AR value is also mainly above 0.2. Tensile failure occurs during the whole loading process. However, shear failure mainly occurs at the unstable crack propagation stage. In addition, the R value falls sharply, and macrocracks occur when shear failure occurs. The distribution of the AR value of specimens at different depths is different, the shear failure of sandstone 113 is less, and no obvious shear failure band is observed. The shear failure band of sandstone 212 occurs only once after the peak strength. The shear failure band of sandstone 333 occurs only once before the peak strength and twice after the peak strength. The shear failure band of sandstone 421 occurs four times before the peak strength and only once after the peak strength. Four shear failure bands occur before the peak strength for sandstone 531, and five shear failure bands occur before the peak strength for sandstone 612. As shown in Fig. 6, the count of the shear failure bands before the peak strength increases gradually, and the count of the shear failure bands after the peak strength increases first and then decreases with burial depth. The main reason is that deep rocks have high in situ stress and rheological properties under higher stress compared with shallow rocks.

Combining the AR value with the peak frequency, there exist some differences in AE characteristics for rock specimens at different depths. During the crack closure stage, elastic deformation stage and crack stable propagation stage, the failure mode is tension cracking. The peak frequency of shallow rocks is mainly at low frequency, while the deep rocks are at high frequency. At the unstable crack propagation stage, the failure mode is tension and shear cracks. The peak frequency of shallow rocks is mainly at high and low frequencies, while the deep rocks are at high, intermediate and low frequencies.

3.5 Characteristic strength of weakly cemented sandstone at different depths

The crack initiation strength of rock is the beginning point of the stable crack propagation stage. After this point, crack growth needs external load driving, while damage strength is the beginning of the unstable crack propagation stage. After this point, crack growth does not need an external load. As shown in Fig. 7, the AE method (Eberhardt et al. 1998; Chang and Lee 2004; Diederichs et al. 2004; Zhao et al. 2013, 2015; Kim et al. 2015; Moradian et al. 2016) and the stress–strain curve method (Brace et al. 1966;

Lajtai 1974; Martin and Chandler 1994; Diederichs 2007) were combined to identify the initiation strength, damage strength, and precursory strength (corresponding strength of failure precursor points) of different rock specimens. The normalized characteristic strength and the k value (ratio of initiation strength to damage strength) of rock specimens at different depths are detailed in Table 2. The normalized characteristic strength of rock specimens at different depths is shown in Fig. 8. The high discreteness of the normalized characteristic strength is related to the nonorganic mineral composition, grain size, stress conditions, and general integrity of the rock (Galouei and

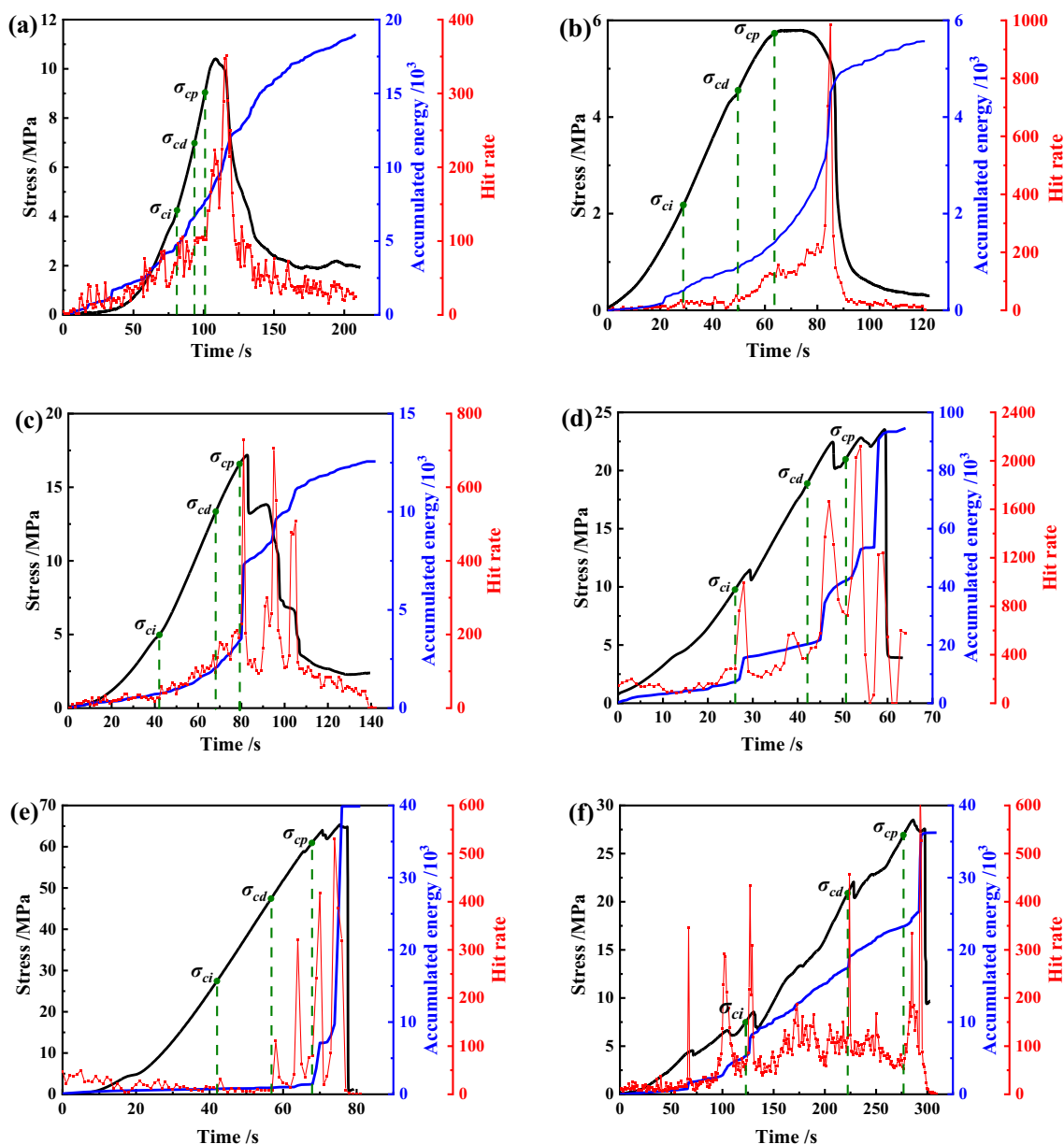


Fig. 7 Curves of AE accumulated energy, hit rate and stress with time of typical rock specimens at different depths **a** specimen 113, **b** specimen 212, **c** specimen 333, **d** specimen 421, **e** specimen 531, **f** specimen 612

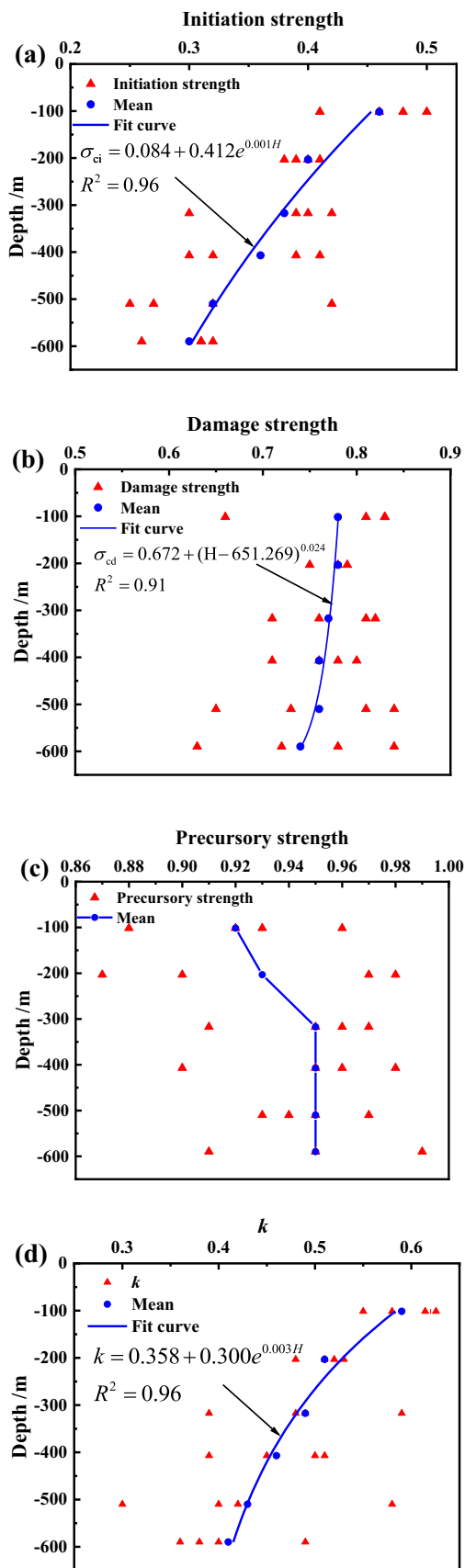
Table 2 Normalized characteristic strength of rock specimens at different depths

Specimen ID	Depth (m)	σ_{ci}/σ_c	σ_{cd}/σ_c	σ_{cp}/σ_c	σ_{ci}/σ_{cd}	Specimen ID	Depth (m)	σ_{ci}/σ_c	σ_{cd}/σ_c	σ_{cp}/σ_c	σ_{ci}/σ_{cd}
111	101.5	0.48	0.83	0.96	0.58	421	406.9	0.41	0.80	0.90	0.51
112	101.5	0.50	0.81	0.93	0.62	422	406.9	0.30	0.76	0.96	0.39
113	101.5	0.41	0.66	0.88	0.62	423	406.9	0.39	0.78	0.98	0.50
114	101.5	0.46	0.83	0.92	0.55	424	406.9	0.32	0.71	0.95	0.45
Mean	–	0.46	0.78	0.92	0.59	Mean	–	0.36	0.76	0.95	0.46
211	203.2	0.39	0.75	0.87	0.52	531	509.9	0.42	0.73	0.93	0.58
212	203.2	0.38	0.79	0.98	0.48	532	509.9	0.25	0.84	0.94	0.30
213	203.2	0.40	0.79	0.97	0.51	533	509.9	0.32	0.81	0.97	0.40
214	203.2	0.41	0.78	0.90	0.53	534	509.9	0.27	0.65	0.95	0.42
Mean	–	0.40	0.78	0.93	0.51	Mean	–	0.32	0.76	0.95	0.43
331	317.3	0.39	0.81	0.91	0.48	611	589.8	0.31	0.63	0.95	0.49
332	317.3	0.40	0.82	0.97	0.49	612	589.8	0.26	0.72	0.95	0.36
333	317.3	0.30	0.76	0.96	0.39	613	589.8	0.32	0.84	0.99	0.38
334	317.3	0.42	0.71	0.95	0.59	614	589.8	0.31	0.78	0.91	0.40
Mean	–	0.38	0.77	0.95	0.49	Mean	–	0.30	0.74	0.95	0.41

Fakhimi 2015), which may be due to the limited number of rock specimens. The average value is a statistic describing the location of a distribution, which can truly to reflect the overall level of data. The distribution of initiation strength ranges from $0.25\sigma_c$ to $0.50\sigma_c$, and the results are consistent with those of Martin and Chandler (1994), Eberhardt et al. (1999) and Zhao et al. (2013, 2015). The average initiation strength of sandstone at 101.5 m is the maximum, which is $0.46\sigma_c$. In contrast, the average initiation strength of sandstone at 589.8 m is the minimum, which is $0.30\sigma_c$, 53.33% ahead of that of sandstone at 101.5 m. On the whole, the initiation strength decreases exponentially with burial depth. The main reason is that the pores and cracks of shallow rocks are relatively developed compared with those of deep rocks, so the corresponding axial P-wave velocity is relatively slow. Therefore, the crack closure stage is relatively long, and the initiation strength is relatively high. With increasing burial depth, the development of internal pores and cracks decreases, the corresponding axial P-wave velocity decreases, the crack closure stage shortens, and the initiation strength decreases. The distribution of damage strength is mainly distributed among the range of 0.63 – 0.84 of σ_c , and the results are consistent with those of Martin and Chandler (1994), Eberhardt et al. (1999), Zhao et al. (2013, 2015), Hidalgo and Nordlund (2013), Kim et al. (2015) and Yang (2016). The average damage strength of sandstone at 101.5 m is $0.78\sigma_c$, while that of sandstone at 589.8 m is $0.74\sigma_c$, which is 5.41% ahead of that of sandstone at 101.5 m. The damage strength decreases as a power function with increasing burial depth as a whole. The main reason is that shallow rocks have relatively higher initiation strength than deep rocks, internal cracks are relatively developed, and the crack

stable propagation stage is relatively long, thus the damage strength is relatively high. With increasing burial depth, the development of internal pores and cracks decreases, and the crack stable propagation stage shortens. Thus, the damage strength decreases.

The distribution of precursory strength (σ_{cp}) ranges from $0.88\sigma_c$ to $0.99\sigma_c$, and the results are consistent with those of Zhao and Jiang (2010). The average precursor strength of sandstone at 101.5 m is $0.92\sigma_c$, while that of sandstone at 589.8 m is $0.95\sigma_c$, which is 3.26% later than that of sandstone at 101.5 m. On the whole, the precursory strength increases with burial depth and tends to be stable after reaching a depth of 300 m. The main reason is that the deep rocks are in a high in situ stress state for a long time and show rheological characteristics under high stress, so the rocks will have long rock dilatancy near the peak strength. Therefore, the precursor strength of deep rocks will be higher and increase with burial depth as a whole. As shown in Fig. 8d, the k value is mainly distributed in the range of 0.30 – 0.62 . The average k value of sandstone at 101.5 m is 0.59, while that of sandstone at 589.8 m is 0.41, which is 43.90% lower than that of sandstone at 101.5 m. Overall, the k value decreases exponentially with burial depth. When the k value is low, the difference between the crack initiation strength and damage strength is high, the crack stable propagation stage is long, and the rock failure is slow. In contrast, when the k value is high, the failure is relatively rapid. Therefore, with increasing mining depth, the possibility of dynamic disasters is greatly increased, and corresponding measures should be taken in advance to prevent dynamic disasters.



◀**Fig. 8** Distribution of normalized characteristic strength and *k* for rock specimens at different depths **a** initiation strength, **b** damage strength, **c** precursory strength, **d** *k*

3.6 Energy evolution of weakly cemented sandstone at different depths

The essence of rock deformation and damage is structural instability driven by energy (Zhang et al. 2015). Therefore, it can be used to analyze the deformation and damage evolution of sandstone at different depths, which is helpful to characterize the mechanical behaviors of sandstone at different depths. As shown in Fig. 9, the input energy mainly accumulates in the form of elastic deformation energy and is released in the form of dissipation energy (Zhang et al. 2019b). In general, the energy is mainly consisted of cumulative input energy, releasable elastic energy, and dissipated energy. As shown in Fig. 9, the cumulative input energy (*U*) can be expressed as

$$U = \int_0^\epsilon \sigma d\epsilon \tag{1}$$

And the releasable elastic energy (*U^e*) can be expressed as:

$$U^e = \frac{\sigma^2}{2E} \tag{2}$$

So the dissipated energy (*U^d*) can be expressed as:

$$U^d = U - U^e \tag{3}$$

According to the stress–strain curves of sandstone at different depths, the three types of energy of sandstone are

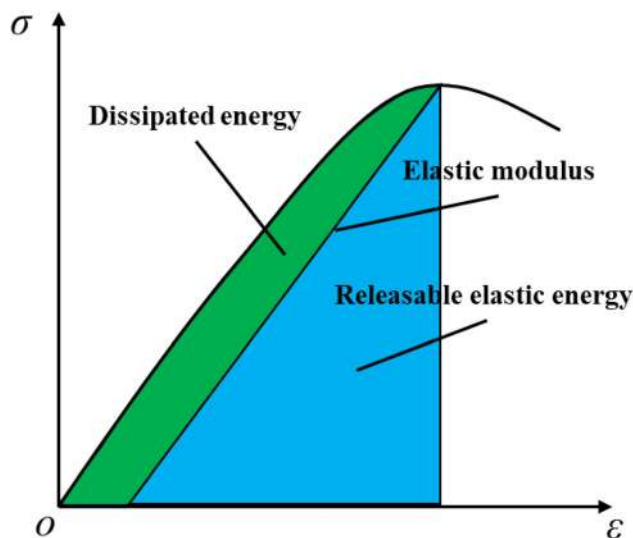


Fig. 9 Calculation method for releasable elastic energy and dissipated energy

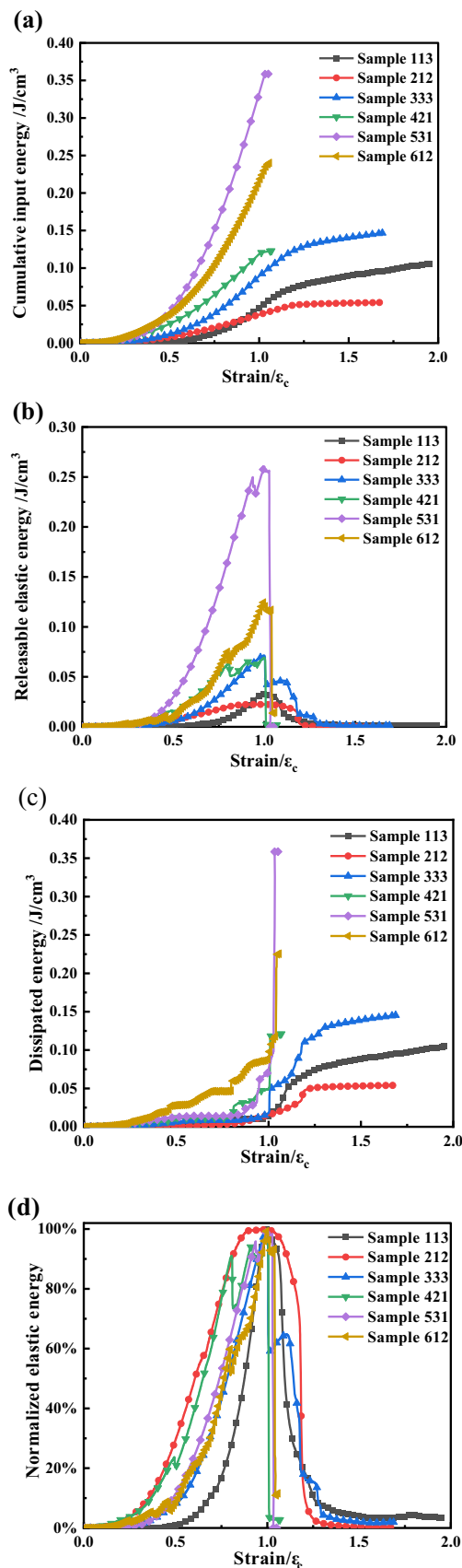


Fig. 10 Energy-strain curves of typical rock specimens at different depths **a** cumulative input energy, **b** releasable elastic energy, **c** dissipated energy, **d** normalized elastic energy

calculated. The energy-strain curves of typical sandstone at different depths are shown in Fig. 10. The cumulative input energy increases linearly with the strain at the prepeak stage and increases slowly at the postpeak stage. In addition, the released elastic energy increases before the peak stress, decreases rapidly near the peak stress and decreases slowly after the peak stress. In contrast, the dissipated energy increases slowly at the prepeak stage, increases rapidly near the peak stress and increases slowly at the postpeak stage. In general, the cumulative input energy, released elastic energy, and dissipated energy increase with depth, reaching maxima of 0.36, 0.26, and 0.36 J/cm³ at a depth of 509.9 m, respectively. Moreover, the cumulative input energy and released elastic energy increase more rapidly with depth at the prepeak stage.

As shown in Fig. 10b and d the elastic energy releases sharply near the peak stress. However, there are some differences between deep sandstone and shallow sandstone. The elastic energy decreases sharply near the peak stress for deep sandstone specimens 421, 531, and 612, while shallow specimens 113, 212, and 333 occur at the postpeak stage. Meanwhile, there is a significant difference between the deep rock and shallow rock in the release rate of elastic energy. The difference in release rate has a great influence on the deformation and failure characteristics. Thus, it is necessary to analyze the release rate of sandstone at different depths. As shown in Fig. 11a, the elastic energy release rate (V_T) is the slope of line CD, and it can be expressed as:

$$V_T = k_{CD} = \frac{U_C^e - U_D^e}{t_D - t_C} = \frac{0.5U_C^e}{t_D - t_C} \quad (4)$$

where U_C^e and U_D^e are the elastic energies of points C and D, respectively, and t_C and t_D are the times of points C and D, respectively.

As shown in Fig. 11b, the release rate ranges from 0.46×10^{-3} to 198.57×10^{-3} J/(cm³ s). The average release rate of sandstone at 203.2 m is 0.94×10^{-3} J/(cm³ s), while that of sandstone at 589.8 m is 167.49×10^{-3} J/(cm³ s), which is 178 times faster than that of sandstone at 203.2 m. Overall, the release rates increase exponentially with burial depth. When the release rate is fast, the possibility and harm of dynamic disasters are greatly increased. Therefore, with increasing mining depth, the possibility of dynamic disasters is greatly increased, and corresponding measures should be taken in advance to prevent dynamic disasters.

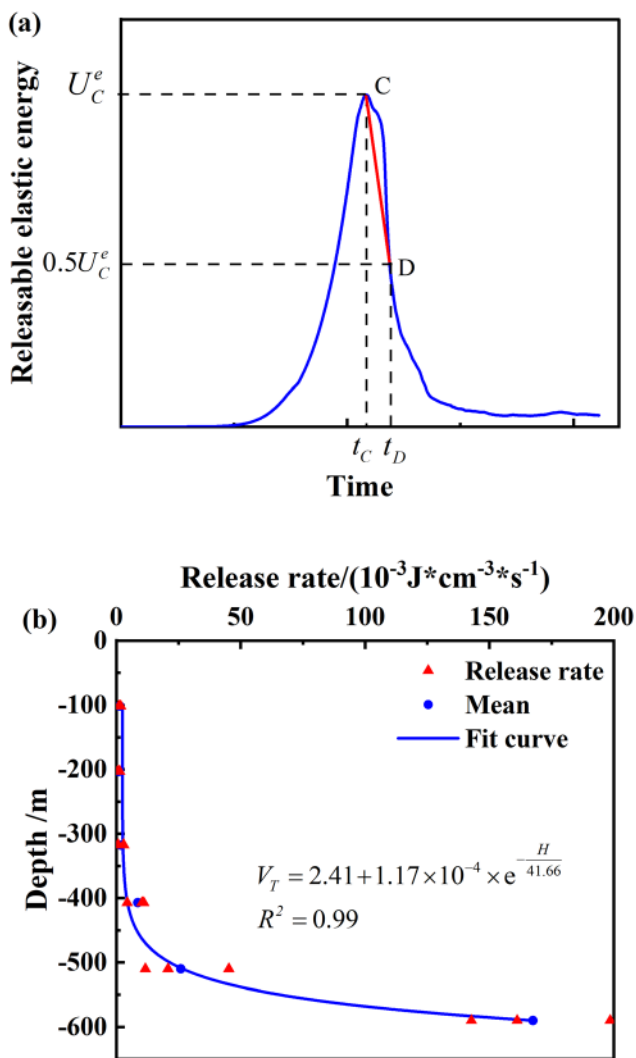


Fig. 11 Definition of elastic energy release rate and distribution of release rate for rock specimens at different depths **a** definition of elastic energy release rate, **b** distribution of release rate

As shallow coal resources are gradually depleted in the western coalfield, resource exploitation extends from shallow to deep depths, where the mechanical properties and deformation behaviors of the rocks change significantly (Xie et al. 2019; Jia et al. 2020). Deep rock shows more complex nonlinear mechanical characteristics due to high geostress, high geotemperature, high permeability and mining disturbance, which cause rock bursts and coal and gas outbursts in deep mining. Moreover, researchers have investigated the physical properties of rock and coal at different depths, such as density, compressive strength, Young’s modulus, Poisson’s ratio, tensile strength, cohesive strength, internal frictional angle, fracture toughness and permeability (Zhou et al. 2010; Song et al. 2016; Man and Liu 2018; Kang et al. 2019; Zhao et al. 2019; Wang et al. 2020), and the mechanical behavior of rock and coal

at different depths, such as AE parameters, energy evolution, damage evolution and failure mechanism (Zhang et al. 2019b; Zhao et al. 2019; Jia et al. 2020). However, research on the characteristic strength, AE and energy evolution of weakly cemented sandstone at different depths is rarely reported. In the present study, the AE method and stress–strain curve method are combined to identify the characteristic strength of weakly cemented sandstone at different depths. The initiation strength and damage strength of sandstone decrease with burial depth, and the main reason is that the pores and cracks of shallow rocks are relatively developed compared with those of deep rocks. In contrast, the precursor strength increases with depth and tends to be stable after reaching a depth of 300 m, and this phenomenon is mainly due to the high in situ stress and high dilatancy in deep rocks. The k value decreases exponentially with depth, indicating that the failure is relatively rapid. Thus, the possibility of dynamic disasters is greatly increased with depth.

Moreover, high geothermal temperature, high in-situ stress, and high pore-water pressure are progressively prominent in the development of deep resources (He et al. 2005; Xie et al. 2019). Underground coal and rock are mainly under triaxial stress, and the confining pressure has significant effects on mechanical properties and deformation characteristics (Xie et al. 2019; Jia et al. 2020). In further studies, the in-situ stress environment and engineering disturbances should be considered in the study of the mechanical behavior and failure pattern of weakly sandstone at different depths.

4 Conclusions

In this study, the characteristic strength, deformation failure characteristics and energy evolution of weakly cemented sandstone at different depths were investigated using uniaxial compression tests. The main findings are as follows.

- (1) The distribution of the peak frequency ranges from 100 to 350 kHz and is mainly concentrated on high and low frequencies, and the intermediate frequency is more intense near the peak strength. The intermediate frequencies of shallow rock specimens mainly occur in the postpeak stage, while deep rock specimens are in the prepeak stage.
- (2) The distribution of initiation strength and damage strength of rock specimens at different depths ranges from $0.23\sigma_c$ to $0.50\sigma_c$ and $0.63\sigma_c$ to $0.84\sigma_c$, respectively, and decreases exponentially and shows a power function with burial depths. The k value of rock specimens ranges from 0.25 to 0.62 and

decreases exponentially with depth. The precursory strength ranges from $0.88\sigma_c$ to $0.99\sigma_c$. The precursor strength increases with depth and tends to stabilize after reaching a depth of 300 m.

- (3) The failure modes of rock specimens with different depths are tension-dominated mixed tensile-shear failure. Shear failure mainly occurs in the unstable crack propagation stage. With increasing burial depth, the count of the shear failure bands before the peak strength increases gradually, and the count of the shear failure bands after the peak strength increases first and then decreases.
- (4) The cumulative input energy, released elastic energy, and dissipated energy increase with depth. The elastic release rate ranges from 0.46×10^{-3} to $198.57 \times 10^{-3} \text{ J}/(\text{cm}^3 \text{ s})$, and the energy release rate increases exponentially with burial depth.

Acknowledgements This work was supported by the National Natural Science Foundation of China (Nos. U1910206, 51874312, 51861145403), Science and Technology Project of Inner Mongolia Autonomous Region (No. 2019GG140), Major Scientific and Technological Innovation Project of Shandong Province (Nos. 2019SDZY01, 2019SDZY02). These sources of supports are gratefully acknowledged.

Author's contributions BL: Writing original draft & Data processing. YZ: Methodology, Review & Editing. CZ: Review & Editing. JZ: Data processing. YL: Data processing. ZS: Data processing.

Declarations

Conflict of interest All the authors of this manuscript have approved the article's submission for publication, and there are no conflicts of interest to declare. This paper has not been published elsewhere and is not under consideration by another journal.

Open Access This article is licensed under a Creative Commons Attribution 4.0 International License, which permits use, sharing, adaptation, distribution and reproduction in any medium or format, as long as you give appropriate credit to the original author(s) and the source, provide a link to the Creative Commons licence, and indicate if changes were made. The images or other third party material in this article are included in the article's Creative Commons licence, unless indicated otherwise in a credit line to the material. If material is not included in the article's Creative Commons licence and your intended use is not permitted by statutory regulation or exceeds the permitted use, you will need to obtain permission directly from the copyright holder. To view a copy of this licence, visit <http://creativecommons.org/licenses/by/4.0/>.

References

- Aggelis DG (2011) Classification of cracking mode in concrete by acoustic emission parameters. *Mech Res Commun* 38:153–157. <https://doi.org/10.1016/j.mechrescom.2011.03.007>
- Aldahdooh MAA, Bunnori NM (2013) Crack classification in reinforced concrete beams with varying thicknesses by mean

- of acoustic emission signal features. *Constr Build Mater* 45:282–288. <https://doi.org/10.1016/j.conbuildmat.2013.03.090>
- Brace WF, Paulding JBW, Scholz C (1966) Dilatancy in the fracture of crystalline rocks the jacketing. *J Geophys Res* 71:3939–3953
- Byun YS, Sagong M, Kim SC et al (2012) A study on using acoustic emission in rock slope with difficult ground - focused on rainfall. *Geosci J* 16:435–445. <https://doi.org/10.1007/s12303-012-0035-2>
- Cai M, Kaiser PK, Tasaka Y et al (2004) Generalized crack initiation and crack damage stress thresholds of brittle rock masses near underground excavations. *Int J Rock Mech Min Sci* 41:833–847. <https://doi.org/10.1016/j.ijrmms.2004.02.001>
- Carpinteri A, Corrado M, Lacidogna G (2013) Heterogeneous materials in compression: correlations between absorbed, released and acoustic emission energies. *Eng Fail Anal* 33:236–250. <https://doi.org/10.1016/j.engfailanal.2013.05.016>
- Chang SH, Lee CI (2004) Estimation of cracking and damage mechanisms in rock under triaxial compression by moment tensor analysis of acoustic emission. *Int J Rock Mech Min Sci* 41:1069–1086. <https://doi.org/10.1016/j.ijrmms.2004.04.006>
- Chang SH, Seto M, Lee CI (2001) Damage and fracture characteristics of kimachi sandstone in uniaxial compression. *Geosystem Eng* 4:18–26. <https://doi.org/10.1080/12269328.2001.10541163>
- Diederichs MS (2007) The 2003 Canadian geotechnical colloquium: mechanistic interpretation and practical application of damage and spalling prediction criteria for deep tunnelling. *Can Geotech J* 44:1082–1116. <https://doi.org/10.1139/T07-033>
- Diederichs MS, Kaiser PK, Eberhardt E (2004) Damage initiation and propagation in hard rock during tunnelling and the influence of near-face stress rotation. *Int J Rock Mech Min Sci* 41:785–812. <https://doi.org/10.1016/j.ijrmms.2004.02.003>
- Dou L, Ke Y, Xiaolou C (2021) Fracture behavior and acoustic emission characteristics of sandstone samples with inclined precracks. *Int J Coal Sci Technol* 8(1):77–87
- Eberhardt E, Stead D, Stimpson B, Read RS (1998) Identifying crack initiation and propagation thresholds in brittle rock. *Can Geotech J* 35:222–233
- Eberhardt E, Stimpson B, Stead D (1999) Effects of grain size on the initiation and propagation thresholds of stress-induced brittle fractures. *Rock Mech Rock Eng* 32:81–99
- Elfergani HA, Pullin R, Holford KM (2013) Damage assessment of corrosion in prestressed concrete by acoustic emission. *Constr Build Mater* 40:925–933. <https://doi.org/10.1016/j.conbuildmat.2012.11.071>
- Fan Y, Lu W, Zhou Y et al (2016) Influence of tunneling methods on the strainburst characteristics during the excavation of deep rock masses. *Eng Geol* 201:85–95. <https://doi.org/10.1016/j.enggeo.2015.12.015>
- Galouei M, Fakhimi A (2015) Computers and geotechnics size effect, material ductility and shape of fracture process zone in quasi-brittle materials. *Comput Geotech* 65:126–135. <https://doi.org/10.1016/j.compgeo.2014.12.010>
- Hall SA, de Sanctis F, Viggiani G (2006) Monitoring fracture propagation in a soft rock (Neapolitan Tuff) using acoustic emissions and digital images. *Pure Appl Geophys* 163:2171–2204. <https://doi.org/10.1007/s00024-006-0117-z>
- He M, Xie H, Peng S, Jiang Y (2005) Study on rock mechanics in deep mining engineering. *Chin J Rock Mech Eng* 24:2803–2813
- Hidalgo KP, Nordlund E (2013) Comparison between stress and strain quantities of the failure–deformation process of Fennoscandian hard rocks using geological information. *Rock Mech Rock Eng* 46:41–51. <https://doi.org/10.1007/s00603-012-0242-1>
- Hoek E, Bieniawski ZT (1965) Brittle rock fracture propagation in rock under compression. *Int J Fract Mech* 1:137–155
- Jia Z, Xie H, Zhang R et al (2020) Acoustic emission characteristics and damage evolution of coal at different depths under triaxial

- compression. *Rock Mech Rock Eng* 53:2063–2076. <https://doi.org/10.1007/s00603-019-02042-w>
- Ju J, Xu J, Zhu W (2015) Longwall chock sudden closure incident below coal pillar of adjacent upper mined coal seam under shallow cover in the Shendong coalfield. *Int J Rock Mech Min Sci* 77:192–201. <https://doi.org/10.1016/j.ijrmms.2015.04.004>
- Kang P, Zhaopeng L, Quanle Z et al (2019) Static and dynamic mechanical properties of granite from various burial depths. *Rock Mech Rock Eng* 52:3545–3566. <https://doi.org/10.1007/s00603-019-01810-y>
- Kim J, Lee K, Cho W et al (2015) A comparative evaluation of stress–strain and acoustic emission methods for quantitative damage assessments of brittle rock. *Rock Mech Rock Eng* 48:495–508. <https://doi.org/10.1007/s00603-014-0590-0>
- Lajtai EZ (1974) Brittle fracture in compression. *Int J Fract* 10:525–536
- Li H, Li H (2017) Mechanical properties and acoustic emission characteristics of thick hard roof sandstone in Shendong coal field. *Int J Coal Sci Technol* 4:147–158. <https://doi.org/10.1007/s40789-017-0163-4>
- Li H, Wang K, Li H, Liu C (2018) Study on mechanical and acoustic emission characteristics of weakly cementation sandstone in Shendong coal field. *Caikuang Yu Anquan Gongcheng Xuebao/j Min Saf Eng* 35:843–851. <https://doi.org/10.13545/j.cnki.jmse.2018.04.024>
- Man K, Liu X (2018) Dynamic fracture toughness and dynamic tensile strength of the rock from different depths of beijing datai well. *Adv Civ Eng*. <https://doi.org/10.1155/2018/2567438>
- Martin CD, Chandler NA (1994) The progressive fracture of lac du bonnet granite. *Int J Rock Mech Min Sci Geomech Abstr* 31:643–659
- Martin CD, Christiansson R (2009) Estimating the potential for spalling around a deep nuclear waste repository in crystalline rock. *Int J Rock Mech Min Sci Geomech Abstr* 46:219–228. <https://doi.org/10.1016/j.ijrmms.2008.03.001>
- Moradian Z, Einstein HH, Ballivy G (2016) Detection of cracking levels in brittle rocks by parametric analysis of the acoustic emission signals. *Rock Mech Rock Eng* 49:785–800. <https://doi.org/10.1007/s00603-015-0775-1>
- Ning J, Wang J, Jiang J et al (2017) Estimation of crack initiation and propagation thresholds of confined brittle coal specimens based on energy dissipation theory. *Rock Mech Rock Eng* 51:119–134. <https://doi.org/10.1007/s00603-017-1317-9>
- Song F, Dong YH, Xu ZF et al (2016) Granite microcracks: structure and connectivity at different depths. *J Asian Earth Sci* 124:156–168. <https://doi.org/10.1016/j.jseaes.2016.04.023>
- Wang H, Liu D, Cui Z et al (2016) Investigation of the fracture modes of red sandstone using XFEM and acoustic emissions. *Theor Appl Fract Mech* 85:283–293. <https://doi.org/10.1016/j.tafmec.2016.03.012>
- Wang L, Guo Y, Yang C et al (2020) Mechanical characterization of continental shale in Sichuan Basin of China and its potential impact on reservoir stimulation. *J Nat Gas Sci Eng* 79:103346. <https://doi.org/10.1016/j.jngse.2020.103346>
- Xie HP, Liu JF, Ju Y et al (2011) Fractal property of spatial distribution of acoustic emissions during the failure process of bedded rock salt. *Int J Rock Mech Min Sci* 48:1344–1351. <https://doi.org/10.1016/j.ijrmms.2011.09.014>
- Xie H, Gao M, Zhang R et al (2019) Study on the mechanical properties and mechanical response of coal mining at 1000 m or deeper. *Rock Mech Rock Eng* 52:1475–1490. <https://doi.org/10.1007/s00603-018-1509-y>
- Xue D, Jie Z, Yintong L, Lie G (2020) On the excavation-induced stress drop in damaged coal considering a coupled yield and failure criterion. *Int J Coal Sci Technol* 7(1):58–67
- Yan W, Dai H, Chen J (2018) Surface crack and sand inrush disaster induced by high-strength mining: example from the Shendong coal field, China. *Geosci J* 22:347–357
- Yang S (2016) Experimental study on deformation, peak strength and crack damage behavior of hollow sandstone under conventional triaxial compression. *Eng Geol* 213:11–24. <https://doi.org/10.1016/j.enggeo.2016.08.012>
- Zhang D, Fan G, Ma L, Wang X (2011) Aquifer protection during longwall mining of shallow coal seams: a case study in the Shendong Coalfield of China. *Int J Coal Geol* 86:190–196. <https://doi.org/10.1016/j.coal.2011.01.006>
- Zhang P, Mishra B, Heasley KA (2015) Experimental investigation on the influence of high pressure and high temperature on the mechanical properties of deep reservoir rocks. *Rock Mech Rock Eng* 48:2197–2211. <https://doi.org/10.1007/s00603-015-0718-x>
- Zhang S, Wu S, Chu C et al (2019a) Acoustic emission associated with self-sustaining failure in low-porosity sandstone under uniaxial compression. *Rock Mech Rock Eng* 52:2067–2085. <https://doi.org/10.1007/s00603-018-1686-8>
- Zhang Z, Xie H, Zhang R et al (2019b) Deformation damage and energy evolution characteristics of coal at different depths. *Rock Mech Rock Eng* 52:1491–1503. <https://doi.org/10.1007/s00603-018-1555-5>
- Zhao Y, Jiang Y (2010) Acoustic emission and thermal infrared precursors associated with bump-prone coal failure. *Int J Coal Geol* 83:11–20. <https://doi.org/10.1016/j.coal.2010.04.001>
- Zhao XG, Cai M, Wang J, Ma LK (2013) Damage stress and acoustic emission characteristics of the Beishan granite. *Int J Rock Mech Min Sci* 64:258–269. <https://doi.org/10.1016/j.ijrmms.2013.09.003>
- Zhao XG, Cai M, Wang J et al (2015) Objective determination of crack initiation stress of brittle rocks under compression using AE measurement. *Rock Mech Rock Eng* 48:2473–2484. <https://doi.org/10.1007/s00603-014-0703-9>
- Zhao Y, Liu B, Yang Z et al (2019) Tensile strength and fracture toughness of sedimentary rocks at different buried depths in Shendong coal field. *J China Coal Soc* 44:1732–1741
- Zhou H, Xie H, Zuo J et al (2010) Experimental study of the effect of depth on mechanical parameters of rock. *Chin Sci Bull* 55:3276–3284
- Zhu W, Xu J, Li Y (2017) Mechanism of the dynamic pressure caused by the instability of upper chamber coal pillars in Shendong coalfield, China. *Geosci J* 21:729–741
- Zhuo H, Qin B, Shi Q, Li L (2018) Development law of air leakage fractures in shallow coal seams: a case study in the Shendong Coalfield of China. *Environ Earth Sci* 77:772. <https://doi.org/10.1007/s12665-018-7961-x>